ARTICLE OPEN

CXCR4-modification enhances CAR-T efficacy by improving tumor tracking and bone marrow homing in B-cell malignancies

Pei Shu[1,2], Fuchun Guo[2,3], Diyuan Qin[2,3], Liqun Zou[4], Qizhi Ma[2], Benxia Zhang[2,3], Ge Gao[2,3], Yue Chen[2,3], Xia He[3,5], Ming Jiang[4], Ning Liu[2], Kexun Zhou[1], Jian Zhao[2], Yanna Lei[2], Yu Gao[2], Yugu Zhang[2], Yao Zeng[2], Mingyang Feng[1], Xiaoyu Li[2,3], Dan Li[6]✉ and Yongsheng Wang[2,5]✉

Hematological malignancies of B cell origin are characterized by frequent expression of CXCR4. The CXCR4-CXCL12 axis facilitates the in vivo dissemination of B cell lymphoma and multiple myeloma (MM). It is also a pivotal regulator in the migration and bone marrow homing of T cells. Herein, we hypothesized that engineering CAR-T cells to overexpress CXCR4 could utilize the CXCR4-CXCL12 axis to enhance their therapeutic efficacy by increasing tumor tracking and bone marrow accumulation. In this study, we found that lentiviral transduction caused significant CXCR4 downregulation on T cells, leading to impaired CAR-T cell migration to CXCL12. By contrast, CXCR4 overexpressing ($CXCR4^{hi}$) CD19 CAR-T cells and BCMA CAR-T cells showed superior in vivo tumor tracking and clearance capacities in the localized and systemically disseminated models of B cell lymphoma and MM, respectively. Notably, *CXCR4* modification significantly facilitated the bone marrow homing and accumulation of CAR-T cells, which further promoted memory T cell differentiation, persistence and prolonged antitumor activity. Building on these findings, an investigator-initiated clinical trial (IIT) evaluating $CXCR4^{hi}$ CD19 CAR-T cells in patients with relapsed/refractory B cell malignancies (NCT04684472) achieved encouraging efficacy: the low-dose cohort yielded 3 complete responses (CRs) and 1 partial response (PR) within the first month post-infusion. These findings support the use of *CXCR4* modification as a strategy to improve CAR-T cell efficacy in treating hematologic B cell malignancies, warranting further clinical investigation.

Signal Transduction and Targeted Therapy (2026)11:38 ; https://doi.org/10.1038/s41392-025-02522-2

INTRODUCTION

Chemokines and their receptors are critical regulators in leukocyte migration and infiltration.[1] The efficient trafficking of CAR-T cells into the tumor site also relies on the match between chemokine receptors on T cells and chemokines secreted by tumors.[2–5] The CXCL12-CXCR4 axis is one of the most conserved and widely expressed chemokine receptor-ligand pairs, playing a non-redundant role in hematopoietic stem cell homing, organ development, and tumor-stromal interactions. It is worth noting that CXCR4-CXCL12 is a crucial signaling axis for both lymphocyte migration and tumor metastasis.[6,7] Within the tumor microenvironment, CXCL12 recruits not only $CXCR4^+$ T cells but also $CXCR4^+$ malignant B cells, indicating that both T lymphocytes and tumor cells tend to accumulate in CXCL12-abundant sites.[8] In particular, CXCR4 is broadly expressed on primary B cell lymphoma and multiple myeloma (MM) cells from patients, while its ligand, CXCL12 (also called SDF-1α), is highly expressed in the tissues and organs to which tumor cells frequently disseminate, such as the bone marrow, secondary lymphoid tissues, and liver.[9–12] This axis can be hijacked by malignant B cells, facilitating their trafficking and retention within the bone marrow microenvironment, where they proliferate and evade conventional therapies. This intricate crosstalk between tumor cells and stromal microenvironment underscores the pivotal role of CXCR4-CXCL12 in the disease progression and relapse of B-cell malignancies. On the basis of these findings, we speculated that CXCR4 overexpression on CAR-T cells could potentially promote their infiltration into the CXCL12-enriched tumor sites and organs and simultaneously endow CAR-T cells with enhanced capacities to track and eradicate metastatic $CXCR4^+$ tumor cells.

The in vivo persistence of CAR-T cells, particularly their T cell memory phenotype, is crucial for the clinical success of adoptive T cell therapy.[13–15] Of note, the bone marrow acts as a critical physiological niche for the in vivo differentiation and long-term maintenance of memory T cells.[16,17] Specifically, bone marrow selectively recruits and retains T cells of the central memory (T_{CM})

[1]Division of Abdominal Tumor Multimodality Treatment, Cancer Center, West China Hospital, Sichuan University, Chengdu, People's Republic of China; [2]Division of Thoracic Tumor Multimodality Treatment, Cancer Center, West China Hospital, Sichuan University, Chengdu, People's Republic of China; [3]Clinical Trial Center, West China Hospital, Sichuan University, Chengdu, People's Republic of China; [4]Division of Head & Neck Tumor Multimodality Treatment, Cancer Center, West China Hospital, Sichuan University, Chengdu, People's Republic of China; [5]NMPA Key Laboratory for Clinical Research and Evaluation of Innovative Drug, West China Hospital, Sichuan University, Chengdu, People's Republic of China and [6]Department of Pulmonary and Critical Care Medicine, Institute of Respiratory Health, State Key Laboratory of Respiratory Health and Multimorbidity, Frontiers Science Center for Disease-related Molecular Network, Sichuan Provincial Engineering Laboratory of Precision Medicine, Precision Medicine Key Laboratory of Sichuan Province, West China Hospital, Sichuan University, Chengdu, People's Republic of China
Correspondence: Dan Li (lidan@wchscu.cn) or Yongsheng Wang (wangys@scu.edu.cn)
These authors contributed equally: Pei Shu, Fuchun Guo, Diyuan Qin, Liqun Zou

Received: 6 October 2024 Revised: 5 September 2025 Accepted: 25 November 2025
Published online: 28 January 2026

phenotype among all transferred cells, and simultaneously, creating a supportive microenvironment for the proliferation and self-renewal of these cells.[16,18] Once they home to the bone marrow, T cells not only display enhanced memory differentiation and in vivo expansion but also show increased therapeutic efficacy in mouse tumor model.[16] The bone marrow niche provides a unique cytokine-rich microenvironment (for example, IL-7 and IL-15) which is critical for T cell survival and homeostatic expansion. This niche also facilitates the direct cell-cell contacts that help preserve T cells in a stem cell-like state with reduced differentiation, which is associated with their rapid effector function upon antigen re-exposure.[17] Considering the pivotal role of CXCR4-CXCL12 in T cell bone marrow homing and elevated CXCL12 level in the tumor microenvironment of B cell lymphoma and MM, we speculated that CXCR4 expression on CAR-T cells could be important for their in vivo memory cell differentiation and therapeutic efficacy.[18–21]

In humans, T lymphocytes constitutively express chemokine receptor CXCR4, which regulates T cell migration toward the CXCL12 gradient.[22] However, decreased surface CXCR4 expression in T cells was observed post-activation by anti-CD3 mAbs or antigen stimulation.[23,24] In addition, the current standard manufacturing process for ex vivo CAR-T cell production includes T cell activation and genetic modification; both of these steps can inevitably dampen CXCR4 expression on CAR-T cells, leading to reduced migration in response to CXCL12. And reduced bone marrow homing was also a potential cause for the impaired antitumor efficiency of CAR-T cells in hematologic malignancy, due to the ineffective clearance of bone marrow-infiltrating tumor cells.[25] Furthermore, human immunodeficiency virus-1 (HIV-1)-based lentiviral transduction is the prevailing approach for gene transfer during CAR-T cell manufacturing.[26] In fact, HIV-1 infection-induced CXCR4 downregulation has been reported by different groups.[27–29] Like HIV-1, lentiviruses also contain elements such as Tat that can mediate the downregulation of T cell surface CXCR4.[30] Therefore, to utilize the CXCR4-CXCL12 axis for efficient bone marrow homing and CXCL12^{+} tumor tracking, it is necessary to reinforce the CXCR4 expression on CAR-T cells.

In this study, we reported that during CAR-T cell manufacturing, surface CXCR4 expression was remarkably downregulated in the CAR^{+} T cells after lentivirus-mediated gene transduction, which consequently leading to impaired chemotactic response to CXCL12. By contrast, the enforced CXCR4 expression (CXCR4^{hi}) of CAR-T cells via genetic modification significantly enhanced their in vivo tumor tracking and bone marrow homing capacities. In both the localized and systemically disseminated models of B-cell lymphoma and MM, CXCR4^{hi} CAR-T cells demonstrated superior therapeutic efficacy when compared to their second-generation counterparts, even at a quarter of the infusion dose. More importantly, with improved bone marrow homing and accumulation, *CXCR4*-modified CAR-T cells showed sustained immune protection and enhanced in vivo memory T cell differentiation. On the basis of these findings, a first-in-human clinical trial of autologous CXCR4^{hi} CD19 CAR-T cells was conducted in patients with relapsed/refractory (r/r) B-cell lymphoma (NCT04684472).

RESULTS

Lentivirus-mediated gene transduction downregulates CXCR4 expression on the T cell surface

To investigate the potential influence of lentiviral transduction on CXCR4 expression, healthy donor-derived T cells were transfected with a second-generation CD19-targeted CAR. Compared with the anti-CD3/CD28 bead-stimulated untransduced (UTD) counterpart, a prominent reduction in cell-surface CXCR4 was observed in CD19 CAR^{+} T cells, and there was no discernible disparity between the CD4^{+} and CD8^{+} subsets (Fig. 1a). Furthermore, the dynamic change in CXCR4 expression was evaluated in CD19 CAR^{+} T cells at different time points post-transduction. CXCR4 reduction occurred as early as 6 h post transduction and lasted for over 7 days. Although there was a tendency for recovery, the CXCR4 level remained significantly lower than the pre-transduction baseline level (Fig. 1b). To investigate whether this occurred in T cells transfected with lentiviruses encoding other genes, healthy donor-derived T cells were transduced to express either green fluorescent protein (GFP) or a second-generation BCMA CAR, and a prominent reduction in surface CXCR4 expression was observed on both the GFP^{+} and BCMA CAR^{+} T cells at 72 h post transduction (Fig. 1c). To characterize the underlying mechanism, T cell surface CXCR4 was labeled with FabFluor-pH Red and monitored continuously for 16 h after transduction. The red fluorescence area was markedly increased on T cells, indicating that CXCR4 was redistributed from the cell surface to intracellular compartments (Fig. 1d). This finding was also supported by previous studies showing that HIV-1 infection induced CXCR4 internalization in T cells.[27,31]

On the basis of the above findings, we generated *CXCR4*-modified CAR-T cells via lentiviral co-delivery of a second-generation CD19 CAR and human CXCR4 via a tandem construct (Fig. 1e and Supplementary Fig. 1). Compared with CD19 CAR-T cells, CXCR4^{hi} CD19 CAR-T cells presented significantly elevated and sustained surface CXCR4 expression (Fig. 1f, g). After antigen stimulation, the CXCR4^{hi} CD19 CAR-T cells exhibited a greater rate of proliferation (Fig. 1h, i). Phenotypic analysis revealed comparable compositions of CD4, CD8, and memory T cells, as well as exhausted T cells (Fig. 1j), even in the context of chronic antigen stimulation (Supplementary Fig. 2). Overall, these data showed that lentiviral transduction downregulated surface CXCR4 on T cells, which can be reversed by *CXCR4* modification, resulting in increased proliferation but not phenotypic alterations.

CXCL12 is highly expressed in B cell lymphoma, and *CXCR4*-modified CAR-T cells show enhanced chemotaxis activity

Next, the expression pattern of chemokine genes in human B cell lymphoma was investigated via the Cancer Genome Atlas (TCGA) dataset. By analyzing 40 CCL and CXCL genes, it was noted that CXCL12 was among the most highly expressed genes in human diffuse large B-cell lymphoma (DLBCL) (Fig. 2a and Supplementary Table 1) and compared with normal tissues, DLBCL tissues presented significantly higher CXCL12 mRNA expression (Fig. 2b). Further analysis revealed that high CXCL12 levels were also correlated with shortened life expectancy in DLBCL patients (Fig. 2c). To evaluate the potential influence of CXCR4 on CAR-T cell therapy in clinical settings, CXCR4 expression analysis was conducted on the infusion products of axicabtagene ciloleucel (Axi-cel, FDA-approved autologous CD19 CAR-T cell) via a single-cell transcriptomic dataset (Gene Expression Omnibus database (GEO), GSE208052) that included 7 large B-cell lymphoma (LBCL) patients[32] (Fig. 2d). Compared with that in progressive disease (PD) patients, CXCR4 expression was significantly elevated in the CAR^{+} and memory T cell subsets of complete response (CR) patients (Fig. 2e, f). Our findings indicate that the CXCR4 level in CAR-T cells could be a potential predictor of therapeutic response.

To assess whether *CXCR4* modification endows CAR-T cells with enhanced chemotaxis to CXCL12, in transwell migration assays, UTD-T cells, CD19 CAR-T cells or CXCR4^{hi} CD19 CAR-T cells were cultured in the upper chamber. And the culture medium, rhCXCL12 or the culture supernatant of Raji^{CXCL12} cells was added to the lower chamber (Supplementary Fig. 3). Compared with CD19 CAR-T cells and UTD-T cells, CXCR4^{hi} CD19 CAR-T cells showed superior migration toward CXCL12 gradient (Fig. 2g), indicating that *CXCR4* modification facilitated the enhanced migration of CAR-T cells to CXCL12. Since CXCR4 and CXCL12 are highly conserved in humans and mice,[33] we used tumor-bearing mouse models to investigate whether *CXCR4*-modified CAR-T cells have increased in vivo accumulation in CXCL12-rich

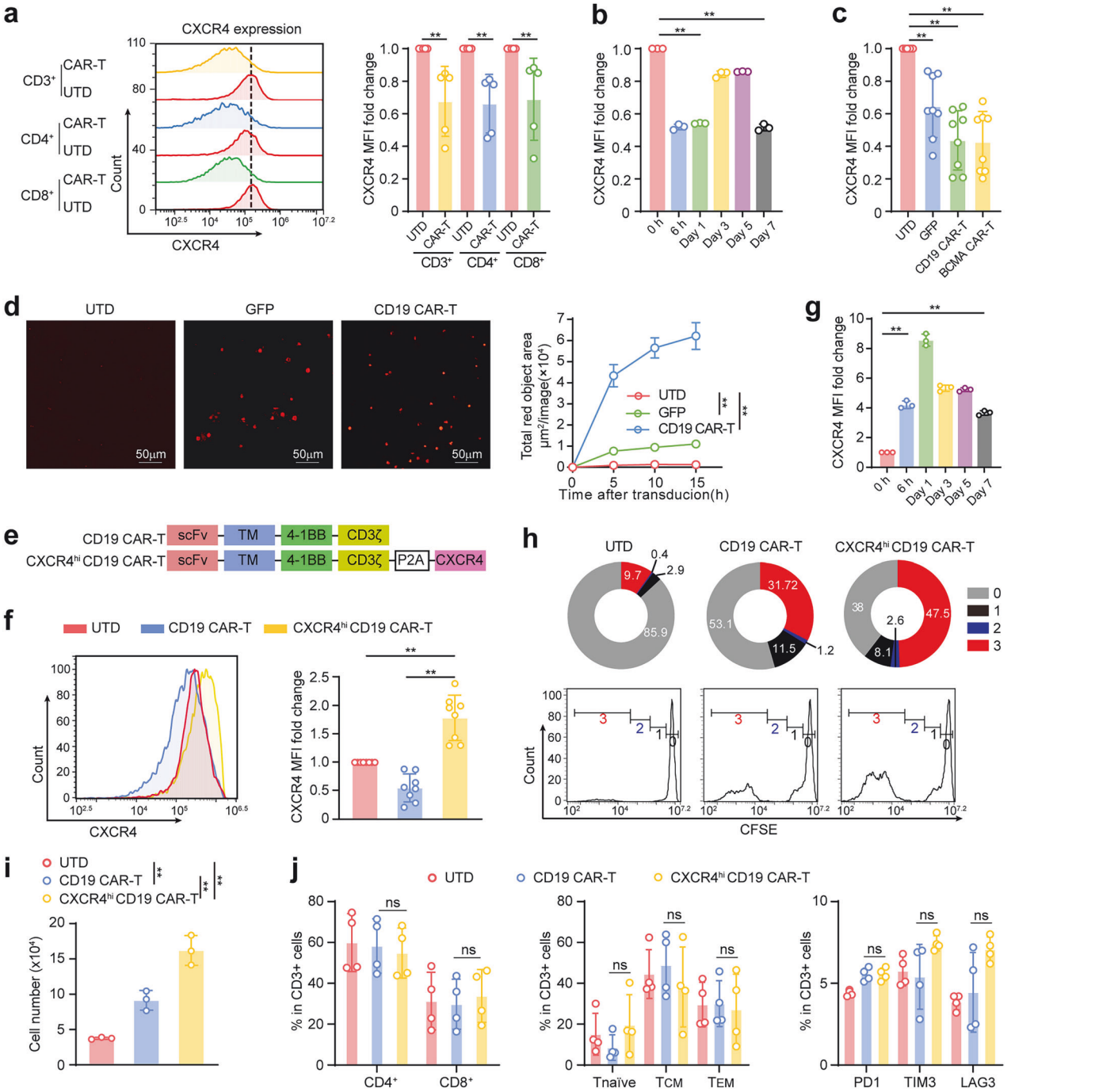

Fig. 1 Lentiviral transduction leads to downregulated surface CXCR4 expression on T cells, which is stably elevated after *CXCR4* modification. **a**–**c** Flow cytometry analysis of surface CXCR4 in lentiviral-transduced T cells from healthy donors. **a** Representative flow cytometry histogram and statistical analysis of the mean fluorescent intensity (MFI) of CXCR4 in $CD3^+$, $CD4^+$ and $CD8^+$ T cell subsets of CD19 CAR^+ and untransduced (UTD)-T cells at 72 h after transduction. $n = 5$ different donors. **b** Changes in the MFI of CXCR4 in CD19 CAR^+ T cells during the 7-day period after transduction. $n = 3$ different donors. **c** CXCR4 MFI in BCMA CAR^+, CD19 CAR^+, GFP^+, and UTD $CD3^+$ T cells at 72 h after transduction. GFP, green fluorescent protein. $n = 8$ different donors. **d** Representative images and analysis of internalized CXCR4 (red) on $CD3^+$ T cells after transduction. **e** Schematic diagram of the human CD19 CAR and $CXCR4^{hi}$ CD19 CAR constructs. **f** Flow cytometry analysis of the surface CXCR4 MFI in CD19 CAR^+, $CXCR4^{hi}$ CD19 CAR^+, and UTD-T cells. $n = 8$ different donors. **g** Flow cytometry analysis of the CXCR4 MFI in $CXCR4^{hi}$ CD19 CAR^+ T cells during the 7-day period after transduction. $n = 3$ different donors. **h** Representative flow cytometry histogram of CFSE-labeled T cells at 24 h poststimulation with irradiated Raji cells. The numbers in the donut charts represent the percentages of each gated fraction. **i** Statistical analysis of the absolute T-cell number at 24 h after antigen stimulation via Precision Count Beads (BioLegend). $n = 3$ different donors. **j** Flow cytometry analysis of CD4, CD8, CD45RO, CD62L, PD1, TIM3 and LAG3 expression in CD19 CAR^+, $CXCR4^{hi}$ CD19 CAR^+, and UTD-T cells. $T_{naïve}$, naïve T cells, $CD45RO^-$ $CD62L^+$; T_{CM}, central memory T cells, $CD45RO^+$ $CD62L^+$; T_{EM}, effector memory T cells, $CD45RO^+$ $CD62L^-$. All the data are presented as the means ± SDs. *p* values were determined via paired *t* tests in **a**–**d**, **f**, **g**, **i**, **j**. $^*p < 0.05$, $^{**}p < 0.01$, ns, not significant

organs. For the Raji^{CXCL12} subcutaneous (s.c.) lymphoma model, mice were intravenously (i.v.) injected with 4×10^6 CD19 CAR-T, CXCR4^{hi} CD19 CAR-T or equivalent UTD-T cells (Fig. 2h). On day 5 after infusion, significantly fewer circulating hCD3$^+$ T cells were detected in the peripheral blood of CXCR4^{hi} CD19 CAR-T cell-treated mice than in that of CD19 CAR-T cell-treated mice (Fig. 2i). In contrast, as early as 24 h after infusion, significantly more hCD3$^+$ T cells were detected in the CXCL12-rich organs (tumor site, spleen and bone marrow) of the CXCR4^{hi} CD19 CAR-T cell groups (Fig. 2i, j). The increase in tumor infiltration was also corroborated

Fig. 2 CXCR4^{hi} CAR-T cells exhibit enhanced in vitro migration toward CXCL12 and increased accumulation within the tumor site and bone marrow. **a** The distribution of mean expression levels for CCL and CXCL family genes (Supplementary Table 1) in diffuse large B-cell lymphoma (DLBCL) cohorts ($n = 48$) from the TCGA database. The solid curve depicts the quantile distribution of CXCL12 across all chemokine genes at each expression level. The dotted line indicates the mean expression of CXCL12. **b** The mRNA expression levels of CXCL12 in human DLBCL and normal tissues were analyzed via the online web server GEPIA (http://gepia2.cancer-pku.cn/#analysis). T, tumor tissue; N, normal tissue. **c** Correlation analysis between disease-free survival (DFS) and CXCL12 levels in DLBCL patients was performed via GEPIA. **d** UMAP plots illustrated distinct T-cell populations and CXCR4 transcripts within CAR$^+$ T cells of infusion products of axicabtagene ciloleucel (Axi-cel) derived from complete response (CR, $n = 5$) or progressive disease (PD, $n = 2$) large B-cell lymphoma (LBCL) patients. Violin plots showing the results of the statistical analysis of CXCR4 expression in all CAR$^+$ T cells (**e**) and memory T cells (**f**). **g** Schematic of the transwell chemotaxis assay (left panel). Percent migration of UTD-T cells, CD19 CAR-T cells, and CXCR4^{hi} CD19 CAR-T cells in response to rhCXCL12 (100 ng/ml) or Raji^{CXCL12} cell culture supernatant (right panel). The number of cells in the lower chamber was determined at 4 h via trypan blue staining. **h** Schematic diagram of the Raji^{CXCL12} s.c. xenograft model. FCM, flow cytometry. **i** Flow cytometry analysis of hCD3$^+$ T cells in the peripheral blood, tumor tissue, bone marrow, and spleen of Raji^{CXCL12} tumor-bearing mice after CAR-T cell infusion. $n = 3$ mice per group. **j** Representative flow cytometry plots. *p* values were determined via Kaplan–Meier analysis in (**c**) and unpaired *t* tests in (**b**, **d**, **e, f**, **g**, **i**, **j**). $^*p < 0.05$, $^{**}p < 0.01$

by IF staining (Supplementary Fig. 4). For other organs, increased accumulation of hCD3$^+$ T cells was also observed in the livers of CXCR4^{hi} CD19 CAR-T cell-treated mice at 24 h post infusion in tumor-free immunodeficient mice (Supplementary Fig. 5). Overall, these data showed that *CXCR4* modification enhanced the in vivo trafficking of CXCR4^{hi} CD19 CAR-T cells and promoted their accumulation at CXCL12-rich sites.

CXCR4-modified CD19 CAR-T cells show enhanced antitumor capacity in B cell lymphoma

To evaluate the in vitro cytotoxicity of *CXCR4*-modified CAR-T cells, CD19$^+$ human B cell lymphoma cell lines (Raji, Daudi, and Ramos) were cocultured with UTD-T cells, CD19 CAR-T cells or CXCR4^{hi} CD19 CAR-T cells in cytokine-free medium for 24 h. K562 cells were used as a negative control (Supplementary Fig. 6). CD19 CAR-T cells and CXCR4^{hi} CD19 CAR-T cells presented comparable cytolytic activities (Fig. 3a), which was also corroborated by the release of effector cytokines, either in the presence or absence of rhCXCL12 (Fig. 3b and Supplementary Fig. 7).

To further investigate whether *CXCR4* modification endows CD19 CAR-T cells with enhanced therapeutic efficiency, mice bearing s.c. implanted Raji^{CXCL12} tumors were i.v. injected with either 4×10^6 CD19 CAR-T cells, CXCR4^{hi} CD19 CAR-T cells or equivalent numbers of UTD-T cells. Given that in B cell lymphoma microenvironment, CXCL12 is abundantly expressed not only by tumor cells but also stromal cells. Raji cells, which normally secrete undetectable levels of CXCL12, were engineered to overexpress CXCL12 (Raji^{CXCL12}) to better mimic the elevated CXCL12 expression that is commonly observed in DLBCL. Compared with CD19 CAR-T cells, CXCR4^{hi} CD19 CAR-T cells showed superior antitumor efficacy and rapidly eradicated Raji^{CXCL12} tumors within 12 days. And durable remission was observed for more than 40 days (Fig. 3c). On the basis of these findings, we proceeded to determine whether a lower dose of CXCR4^{hi} CD19 CAR-T cells could mediate similar antitumor efficacy. Notably, 1×10^6 CXCR4^{hi} CD19 CAR-T cells exhibited a comparable tumor regression capacity as that of 4×10^6 CD19 CAR-T cells and eradicated Raji^{CXCL12} tumors within 15 days (Fig. 3d). The results indicated that the CXCR4^{hi} CD19 CAR-T cells achieved earlier and more potent antitumor efficacy, even at a quarter-dose of their second-generation counterpart.

In B cell lymphoma and MM patients, CXCR4 is the main chemotaxis receptor that mediates tumor cell dissemination to CXCL12-rich organs.[9,12] In DLBCL, high CXCR4 expression is also an independent prognostic factor for decreased survival.[34] Indeed, high surface CXCR4 expression was detected in both human B-cell lymphoma (Raji, Daudi, Ramos, and K562) and MM cells (RPMI 8226 and U266) (Supplementary Fig. 8). Therefore, we hypothesized that the CXCR4-CXCL12 axis could be utilized by CAR-T cells as a tumor-tracking signal to eradicate disseminated malignant cells. A systemically disseminated CD19$^+$ B-cell lymphoma model was established via i.v. injection of Fluc-transduced wild-type Raji (Raji^{luc}) cells. Compared with CD19 CAR-T cells, CXCR4^{hi} CD19 CAR-T cells significantly reduced the disseminated lesions in Raji^{luc}-bearing mice, and 50% (3/6) of the CXCR4^{hi} CD19 CAR-T cell-treated mice achieved complete tumor regression within 2 weeks (Fig. 3e, f). All the mice in CXCR4^{hi} CD19 CAR-T cell group had prolonged overall survival (Fig. 3g). Since CXCR4$^+$ Raji cells tend to migrate to CXCL12-rich organs, the frequency of hCD19$^+$ Raji cells was analyzed on day 14 after infusion, and a significantly lower percentage of hCD19$^+$ cells were detected in the liver and bone marrow of CXCR4^{hi} CD19 CAR-T cell-treated mice (Fig. 3h), which was further validated by H&E staining (Fig. 3i, j). Overall, these data demonstrated that *CXCR4* modification substantially augmented the tumor tracking capacity of CD19 CAR-T cells, resulting in superior elimination of CD19$^+$ B cell lymphoma in vivo.

The bone marrow environment endows *CXCR4*-modified CD19 CAR-T cells with increased memory differentiation ability and long-term immune protection

Previous studies have shown that T cell recruitment to the bone marrow is critically regulated by CXCR4, which enhances memory differentiation as well as the antitumor immunity of therapeutic T cells.[16,35] We also observed an early increase of bone marrow-accumulated T cells in the CXCR4^{hi} CD19 CAR-T cell-treated group (Fig. 2i). To further elucidate how *CXCR4* modification endows CAR-T cells with enhanced function in vivo, bone marrow-infiltrated hCD3$^+$ T cells from Raji^{CXCL12} s.c. tumor-bearing mice were isolated and analyzed at 30 days post infusion. Compared with that in CD19 CAR-T cell-treated mice, there was a ~3-fold increase of bone marrow-accumulated hCD3$^+$ T cells in mice received CXCR4^{hi} CD19 CAR-T cell treatment (Fig. 4a). And this was further corroborated by IF staining (Fig. 4b). In addition, we observed a significantly greater proportion of CD45RO$^+$ CD62L$^+$ central and CD45RO$^+$ CD62L$^-$ effector memory T cells (T_{CM} and T_{EM}) in the bone marrow of these mice (Fig. 4c).

CXCL12 is highly and constitutively expressed by bone marrow stromal cells.[36] To explore the potential influence of CXCL12 on memory T-cell differentiation, CXCR4^{hi} CD19 CAR-T cells and CD19 CAR-T cells were antigen-stimulated and incubated in culture medium containing rhCXCL12 for 24 h. However, unlike bone marrow-infiltrated T cells (Fig. 4c), there was no significant difference in the percentage of memory T cells between the two groups (Supplementary Fig. 9a), which was also corroborated by gene set enrichment analysis (GSEA) (Supplementary Fig. 9b, c). In contrast, transcriptome sequencing of bone marrow-infiltrated hCD3$^+$ T cells confirmed the upregulation of memory T cell-related gene sets in bone marrow-isolated T cells from CXCR4^{hi} CD19 CAR-T cell-treated mice (Fig. 4d, e). These results indicated that it was the bone marrow microenvironment, but not the CXCL12 chemokine alone, mediated the elevated memory T-cell differentiation of CXCR4^{hi} CD19 CAR-T cells. KEGG enrichment analysis

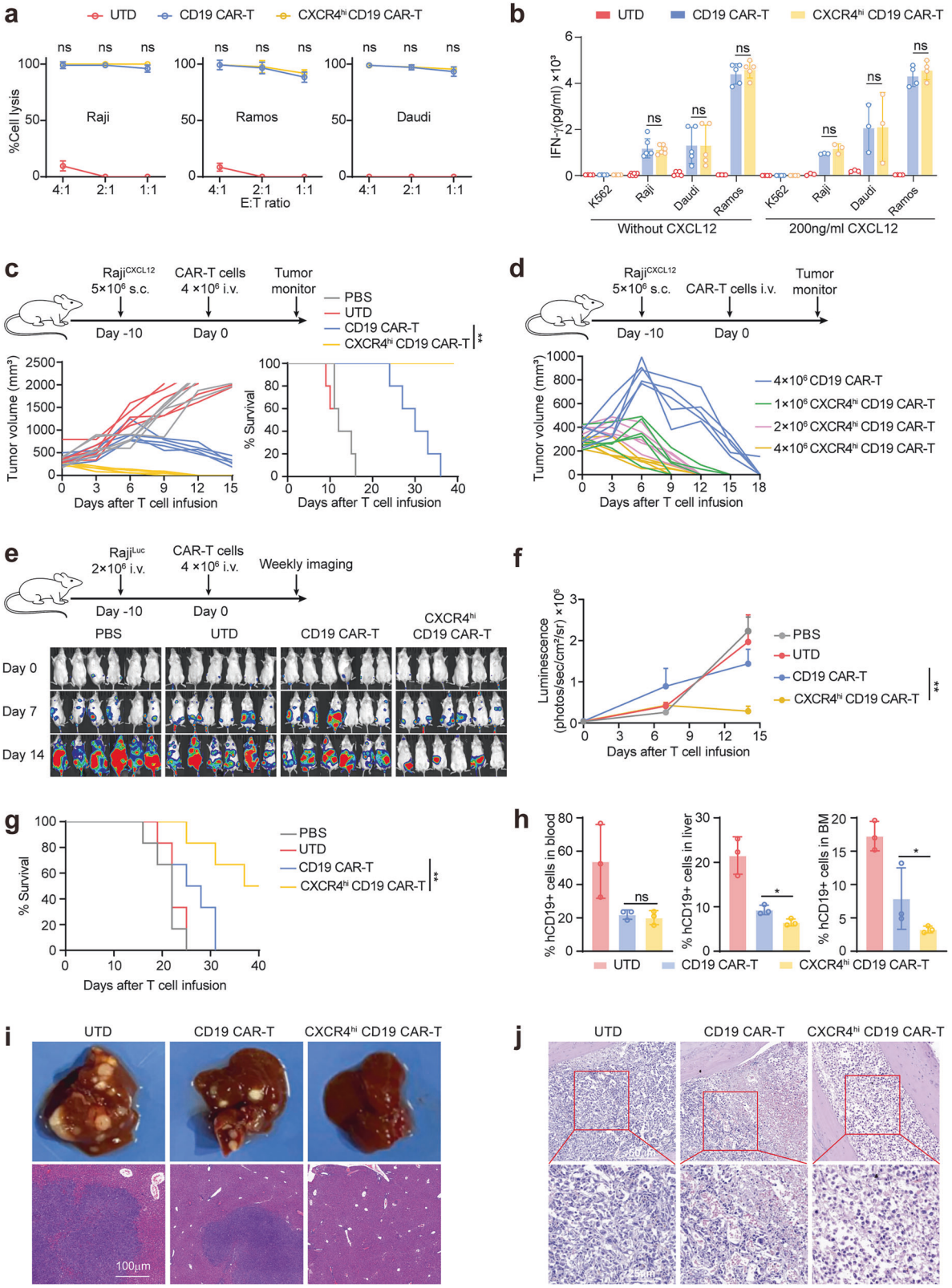

revealed that most DEGs between bone marrow-infiltrated and in vitro cultured CXCR4^{hi} CD19 CAR-T cells were enriched in signaling pathways related to differentiation, activation, and immune response-activating signal transduction (Fig. 4f). RNA-seq also revealed remarkable upregulation of CXCR4 expression in bone marrow-infiltrated CXCR4^{hi} CD19 CAR-T cells compared with their in vitro cultured counterparts (Fig. 4g). Notably, hCD3^{+} T cells isolated from the bone marrow of CXCR4^{hi} CD19 CAR-T cell-treated mice presented downregulated gene sets associated with proliferation, activation, and exhaustion, as compared with those

Fig. 3 CXCR4^{hi} CD19 CAR-T cells exhibit enhanced in vivo antitumor efficacy in B-cell lymphoma. **a** The in vitro cytotoxicities of UTD-T cells, CD19 CAR-T cells, and CXCR4^{hi} CD19 CAR-T cells were analyzed via flow cytometry after 24 h of coincubation with CFSE-labeled Raji, Ramos or Daudi cells. E:T, effector: target. $n = 3$ different donors per group. **b** Statistical analysis of IFN-γ release after 24 h of coincubation with Raji, Daudi, Ramos, or K562 cells (negative control), either in the presence or absence of CXCL12 (200 ng/ml). E: T = 1:1. **c** Tumor growth and survival curves of Raji^{CXCL12} s.c. tumor-bearing mice i.v. injected with 4×10^6 CD19 CAR-T cells, CXCR4^{hi} CD19 CAR-T cells or UTD-T cells. $n = 5$ mice per group. **d** Tumor growth curve of Raji^{CXCL12} s.c. tumor-bearing mice that i.v. injected with either 4×10^6 CD19 CAR-T cells or 1×10^6, 2×10^6, or 4×10^6 CXCR4^{hi} CD19 CAR-T cells. $n = 5$ mice per group. **e** Representative bioluminescence (BLI) images of Raji^{luc} tumor growth in a systemically disseminated model. Raji^{luc} tumor-bearing mice were i.v. injected with 4×10^6 CD19 CAR-T cells, CXCR4^{hi} CD19 CAR-T cells or UTD-T cells. Tumor progression was monitored via an in vivo imaging system (IVIS). **f** Statistical analysis of in vivo fluorescence imaging and **g** survival curves of Raji^{luc} tumor-bearing mice. $n = 6$ mice per group. **h** Quantification of hCD19$^+$ tumor cells in Raji^{luc} systemically disseminated mice at 14 days after T-cell infusion. $n = 3$ mice per group. **i** Representative images (upper) and H&E staining (lower) of liver tissues at 14 days post-T-cell infusion. **j** H&E staining of bone marrow at 14 days post-T-cell infusion. **i, j** Tumor models were established and treated as described in (**e**). The data are presented as the means ± SDs. *p* values were determined via the log-rank Mantel–Cox test in (**c**, **g**) and the unpaired *t* test in (**a**, **b**, **f**, **h**), $^*p < 0.05$, $^{**}p < 0.01$, ns, not significant

of CD19 CAR-T cell-treated mice (Supplementary Fig. 10), further suggesting that in the bone marrow, CXCR4^{hi} CD19 CAR-T cells reside in a quiescent memory state, which is consistent with previous reports.[37,38] Together, these data suggest that the bone marrow microenvironment particularly facilitates the in vivo memory differentiation of CXCR4^{hi} CD19 CAR-T cells.

Furthermore, to evaluate whether CXCR4^{hi} CD19 CAR-T cell treatment exhibits long-term protection against CD19$^+$ Raji tumors, the mice with tumor regression shown in Fig. 3c were reinoculated with parental Raji^{CXCL12} cells. Compared with naïve mice, tumor regression mice presented significantly prolonged survival after rechallenge (Fig. 4h). Overall, the data demonstrated that *CXCR4* modification enhanced the recruitment of CAR-T cells to the bone marrow, leading to the increased in vivo memory T-cell differentiation and prolonged immune protection.

CXCR4-modified BCMA CAR-T cells show enhanced antitumor efficacy in multiple myeloma

To further assess the influence of *CXCR4* modification on CAR-T cells that target other hematological malignancies, CXCR4^{hi} BCMA CAR-T cells were constructed similarly (Supplementary Fig. 11a and Fig. 5a, b). In accordance with CXCR4^{hi} CD19 CAR-T cells, CXCR4^{hi} BCMA CAR-T cells presented significantly enhanced in vitro chemotaxis to rhCXCL12 (Fig. 5c) and comparable cytotoxicity against BCMA$^+$ MM cell lines (RPMI 8226, H929, U266, and OPM2) when compared to second-generation CAR-T cells (Fig. 5d, e, and Supplementary Fig. 11b). To investigate in vivo antitumor efficacy, mice bearing RPMI 8226s.c. tumors were infused with either 5×10^6 UTD-T cells or BCMA CAR-T cells or with 5×10^6, 2.5×10^6 or 1.25×10^6 CXCR4^{hi} BCMA CAR-T cells. Compared with BCMA CAR-T cells, CXCR4^{hi} BCMA CAR-T cells presented superior antitumor efficacy, with comparable eradication rates even when they were infused with a quarter-dose of BCMA CAR-T cells. When infused at the same or half the dose of BCMA CAR-T cells, the CXCR4^{hi} BCMA CAR-T cells induced more rapid tumor regression (Fig. 5f). In the systemically disseminated Fluc-transduced RPMI 8226 (RPMI 8226^{Luc}) tumor model, CXCR4^{hi} BCMA CAR-T cells rapidly eradicated tumor cells within 14 days, and durable remission was noted for more than 60 days after infusion (Fig. 5g–i). Taken together, these data demonstrated that *CXCR4* modification substantially augmented the in vivo antitumor efficacy of BCMA CAR-T cells.

CXCR4-modified CD19 CAR-T cells exhibit encouraging benefits in r/r B-cell lymphoma patients

A first-in-human study (ClinicalTrial.gov, NCT04684472) was conducted to evaluate the safety and efficacy of autologous CXCR4^{hi} CD19 CAR-T cells in relapsed/refractory (r/r) B-cell lymphoma patients (Fig. 6a). In this 3+3 dose-escalation study, four patients with refractory DLBCL (defined as those with less than a complete response to first-line therapy[39]) were enrolled in the cohort receiving 1×10^6 CAR$^+$ T cells/kg. The average transduction efficiency of the infusion products was 48% (range, 22–71.5%), and the CXCR4 MFI of the CAR$^+$ T cells was 3.6-fold (range, 1.60–5.89) greater than that of the UTD-T cells (Supplementary Fig. 12b, c). IFN-γ release detection revealed that DLBCL patient-derived CXCR4^{hi} CD19 CAR-T cells had robust in vitro cytotoxicity against CD19$^+$ tumor cells (Supplementary Fig. 12d).

The four patients received a single dose of CXCR4^{hi} CD19 CAR-T cells ranging from 4.0 to 9.9×10^7 CAR$^+$ T cells (1×10^6 CAR$^+$ T cells/kg; Fig. 6a and Supplementary Tables 2 and 3). One month after infusion, three patients (Pt1, Pt2, and Pt4) achieved a complete response (CR), and the other patient (Pt3) achieved a partial response (PR) (Fig. 6b). Sustained responses were maintained in Pt1, Pt2, and Pt4 at the latest follow-up. Pt3 was lost to follow-up after the initial evaluation and did not undergo reassessment (Fig. 6c). The predominant treatment-emergent adverse events (TEAEs) were leukopenia and anemia (Supplementary Table 4). Grade ≥3 TEAEs occurred most frequently for leukopenia and lymphopenia (Supplementary Table 4). Two patients experienced grade 1 cytokine release syndrome (CRS), and 1 patient experienced immune effector cell-associated neurotoxicity syndrome (ICANS) (Fig. 6d), which occurred within 7 days after infusion and resolved spontaneously within 2–8 days. The circulating CAR level initially peaked between days 14 and 21 post infusion and then subsequently declined (Fig. 6e). Only mild increases in the levels of serum cytokines (IL-2, IL-4, IL-6, IL-10, IL17, IFN-γ, and TNF-α) were detected (Fig. 6f). Together, these data preliminarily suggest that CXCR4^{hi} CD19 CAR-T cells show high therapeutic efficacy and safety in r/r B-cell lymphoma patients at a dose of 1×10^6 CAR$^+$ T cells/kg.

DISCUSSION

Impaired in vivo trafficking and limited persistence are considered the two main mechanisms for tumor escape and relapse following CAR-T cell treatment.[40] In this study, we reported that *CXCR4* modification greatly enhanced the in vivo tumor clearance capacity of CD19 CAR-T cells and BCMA CAR-T cells in B cell lymphoma and MM, respectively. Further investigation revealed that *CXCR4* modification facilitated the in vivo trafficking and accumulation of CAR-T cells in CXCL12$^+$ tumor and bone marrow. Notably, this increased bone marrow homing endows CXCR4^{hi} CAR-T cells with markedly enhanced T cell memory differentiation, enabling prolonged in vivo persistence and antitumor immune protection. More importantly, in CXCL12-rich organs of Raji^{luc} tumor-bearing mice, significantly decreased in vivo hCD19$^+$CXCR4$^+$ Raji cell dissemination was detected in CXCR4^{hi} CD19 CAR-T cell-treated group as compared to CD19 CAR-T cell-treated group. Additionally, in an early-phase clinical trial, *CXCR4*-modified CD19 CAR-T cells exhibited a curative effect at an infusion dose of 1×10^6 CAR$^+$ T cells/kg, and only mild treatment-related toxicity was observed. Therefore, we demonstrated that genetically modifying CAR-T cells to overexpress CXCR4 could

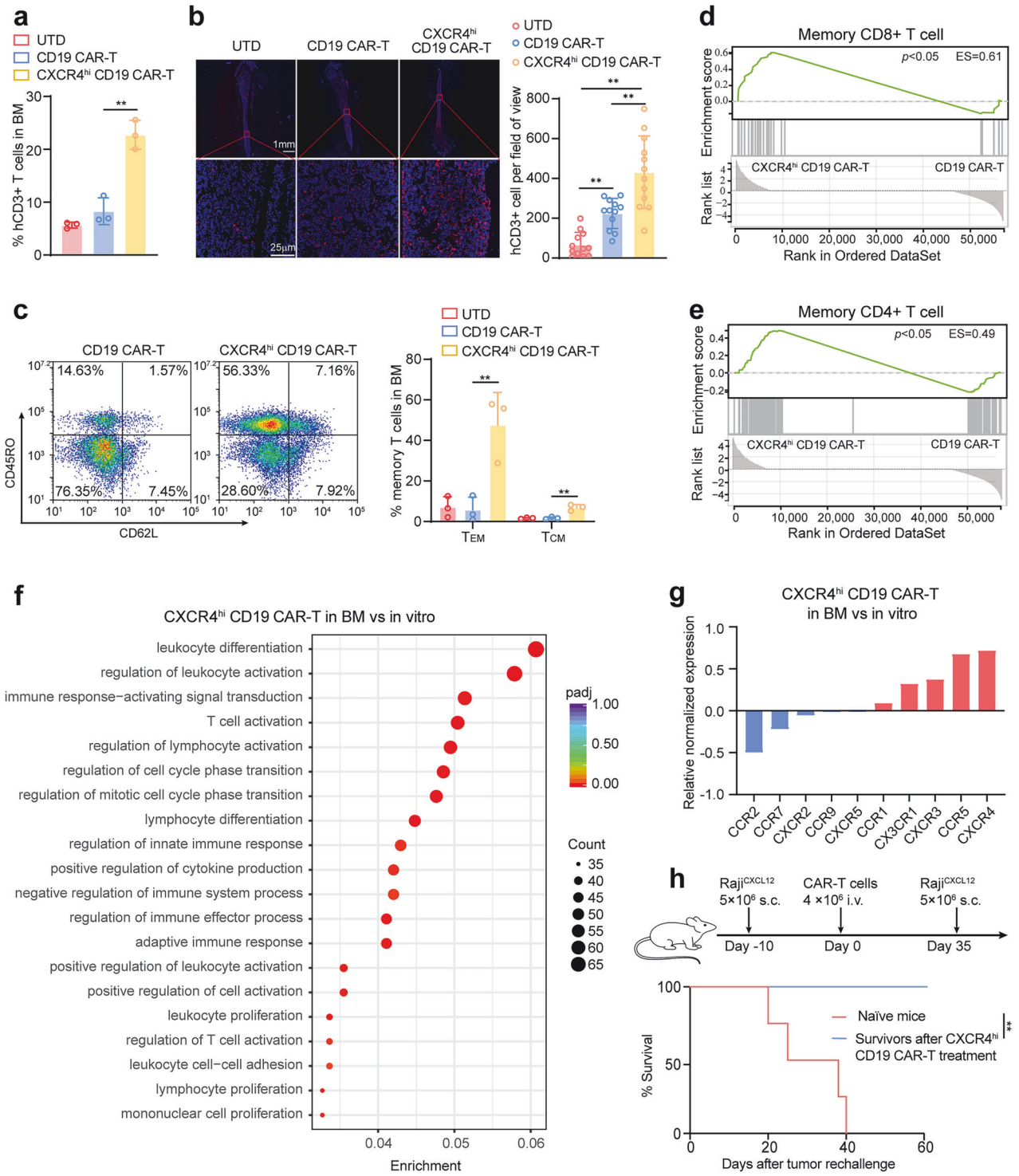

Fig. 4 Increased recruitment of adoptively transferred CXCR4^{hi} CD19 CAR-T cells to the bone marrow (BM) and retention of the memory T cell phenotype. **a**–**g** BM-accumulated CAR-T cells were isolated from Raji^{CXCL12} s.c. tumor-bearing mice by hCD3^{+} sorting at 30 days post-infusion. The tumor model was established and treated as shown in Fig. 3c. **a** Flow cytometry analysis of T cells in the BM. **b** Representative IF images and statistical analysis of BM hCD3 staining (red). **c** Representative flow cytometric plot and statistical analysis of central memory T cells (T_{CM}, CD45RO^{+}CD62L^{+}) and effector memory T cells (T_{EM}, CD45RO^{+}CD62L^{-}) in the BM. **d**, **e** Gene set enrichment analysis (GSEA) of the CD8^{+} and CD4^{+} T-cell memory pathways in BM-infiltrated CXCR4^{hi} CD19 CAR-T cells and CD19 CAR-T cells. **f** KEGG pathway analysis of differentially expressed genes (DEGs) between BM-infiltrated and ex vivo cultured antigen-stimulated CXCR4^{hi} CD19 CAR-T cells from the same batch. **g** Fold changes in the transcription levels of chemokine receptor genes in BM-infiltrated and ex vivo cultured CXCR4^{hi} CD19 CAR-T cells. **h** Tumor rechallenge experiment. The tumor regression mice shown in Fig. 3c and the naïve mice (control) were inoculated s.c. with Raji^{CXCL12} cells (5×10^6). Kaplan–Meier survival analysis was performed. $n = 4$ mice per group. p values were determined via an unpaired t test in (**a**, **c**) and the log-rank Mantel–Cox test in (**h**). *$p < 0.05$, **$p < 0.01$

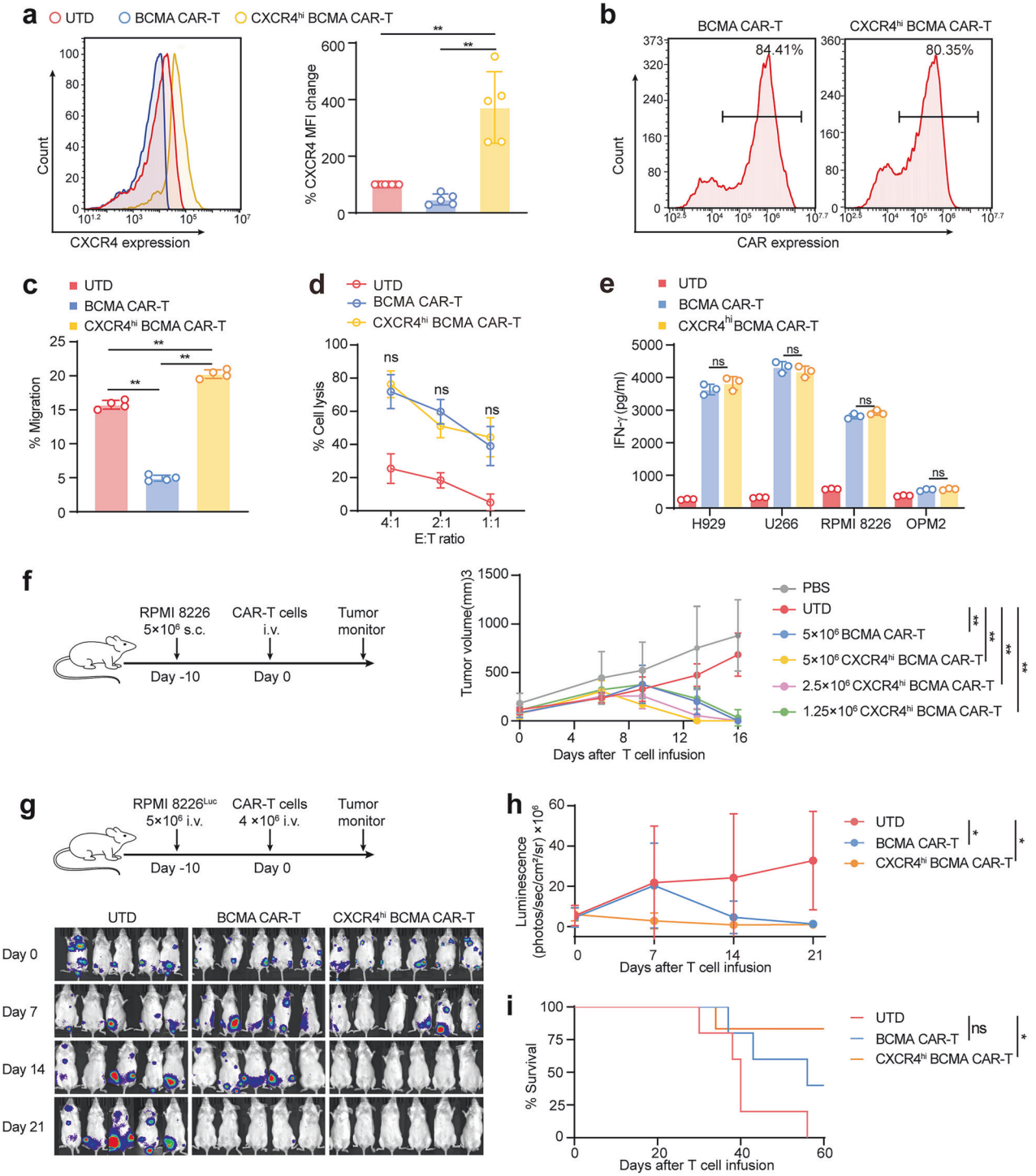

Fig. 5 CXCR4^{hi} BCMA CAR-T cells exhibit enhanced in vivo antitumor efficacy in multiple myeloma. **a** Flow cytometry analysis of CXCR4 expression in BCMA CAR^{+}, CXCR4^{hi} BCMA CAR^{+} and UTD-T cells. $n = 5$ different donors. **b** Representative flow cytometry histogram of BCMA CAR expression in lentiviral-transduced healthy donor-derived CD3^{+} T cells. **c** Percent migration of UTD-T cells, BCMA CAR-T cells, and CXCR4^{hi} BCMA CAR-T cells in response to rhCXCL12 (100 ng/ml). $n = 4$ different donors. **d** The cytotoxicity of CAR-T cells was analyzed by flow cytometry at the indicated E:T ratios after 24 h of coculture with Far Red-labeled RPMI 8226 cells. $n = 3$ different donors. **e** Statistical analysis of IFN-γ released by UTD-T cells, BCMA CAR-T cells, or CXCR4^{hi} BCMA CAR-T cells after coculture with RPMI 8226 cells at an E:T ratio of 1:1 for 24 h. $n = 3$ different donors. **f** Schematic diagram of the RPMI8226 s.c. xenograft model. B-NDG mice were inoculated with RPMI 8226 cells (5×10^6), and 10 days later, they were i.v. injected with 5×10^6 UTD T cells or BCMA CAR-T cells or with 1.25×10^6, 2.5×10^6, or 5×10^6 CXCR4^{hi} BCMA CAR-T cells. Tumor growth was monitored for each group, $n = 5$ mice per group. **g** Schematic diagram of the RPMI8226^{luc} disseminated xenograft model. RPMI8226^{luc} tumor-bearing mice were i.v. injected with 4×10^6 UTD-T cells, BCMA CAR-T cells, or CXCR4^{hi} BCMA CAR-T cells (upper panel). The lower panel shows representative BLI images of RPMI8226^{luc} tumor growth in a systemically disseminated model, and tumor progression was monitored via IVIS. Statistical analysis of in vivo fluorescence imaging and survival curves of RPMI8226^{luc} tumor-bearing mice (**h**, **i**). $n = 5$-6 mice per group. The data are presented as the means ± SDs. p values were determined via the log-rank Mantel–Cox test in (**i**) and the unpaired t test in (**a**, **c**, **d**, **e**, **f**, **h**). *$p < 0.05$, **$p < 0.01$, ns, not significant

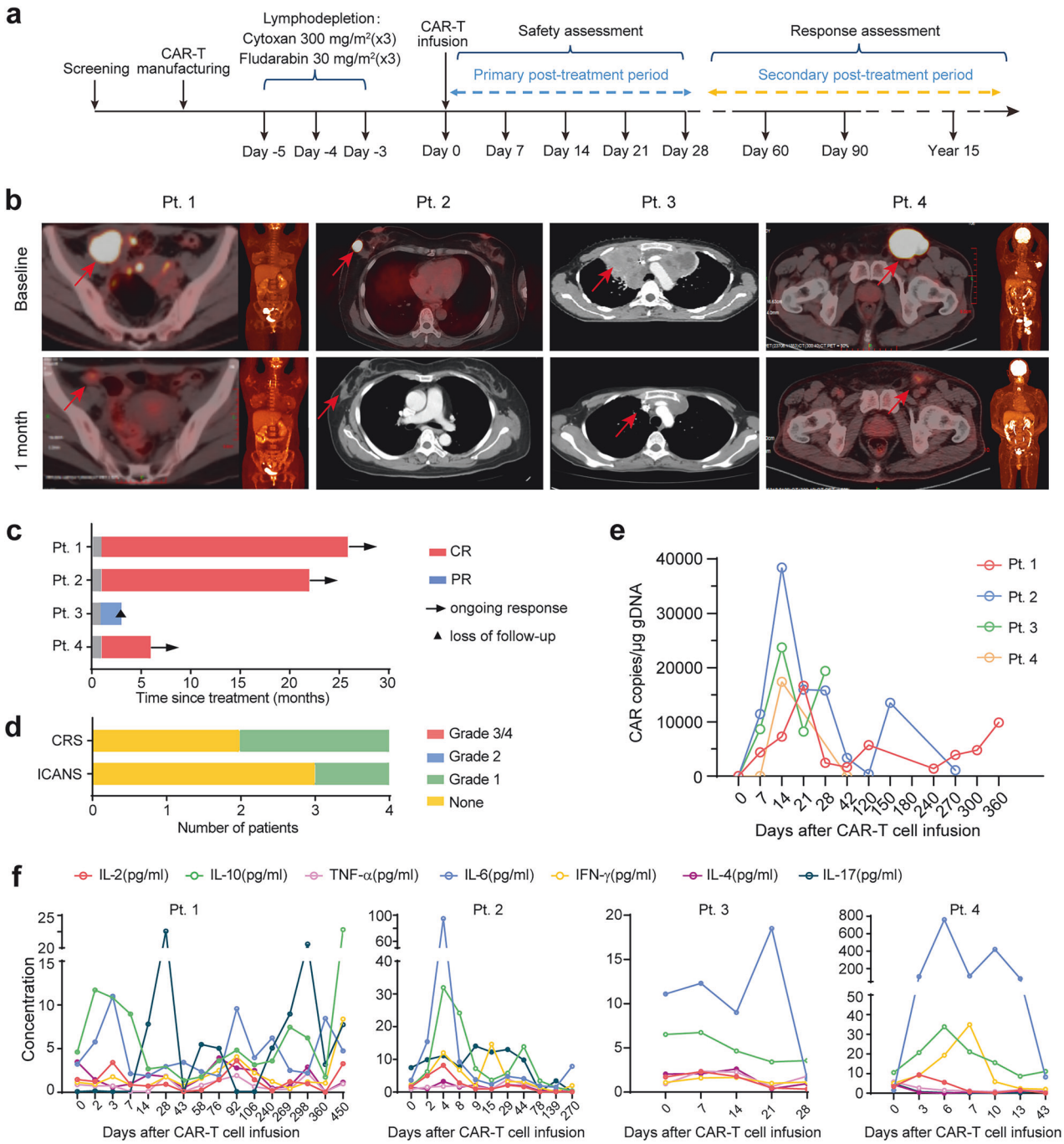

Fig. 6 CXCR4^{hi} CD19 CAR-T cells exhibit potent tumor elimination capacity in patients with r/r B-cell lymphoma and without severe toxicity. **a** Clinical trial schedule. **b** PET/CT and CT scans were performed before and at 1 month after autologous CXCR4^{hi} CD19 CAR-T-cell infusion. **c** Swimmer's plot describing disease status and overall survival for each patient. CR, complete remission. PR, partial response. **d** Adverse events, including cytokine release syndrome (CRS) and immune effector cell-associated neurotoxicity syndrome (ICANS), occurred within the first 4 weeks after CXCR4^{hi} CD19 CAR-T-cell infusion. **e** In vivo persistence of CXCR4^{hi} CD19 CAR-T cells in the peripheral blood was determined by ddPCR and presented as copies/μg of genomic DNA. **f** Serum cytokine levels at different time points after CXCR4^{hi} CD19 CAR-T-cell infusion

leverage the CXCR4–CXCL12 axis to enhance CAR-T cell therapeutic efficacy through improved tumor-targeting and increased bone marrow infiltration.

In this study, we found that lentiviral transduction led to CXCR4 downregulation on T cells via inducing receptor internalization, which was also supported by previous studies showing that HIV-1 infection downregulated T cell surface CXCR4.[27–29] In B cell lymphoma and MM, the CXCR4–CXCL12 axis is involved in multiple key processes related to tumor biological behaviors, including migration, invasion and metastasis.[12,41] *CXCR4* modification not only restores the diminished CXCR4 expression that induced by lentiviral transduction but also strategically generates CAR-T cells that overexpress CXCR4. Notably, CXCR4^{hi} CAR-T cells not only exhibited substantially increased infiltration into CXCL12^{+} tumors but also exhibited superior in vivo tracking to disseminated tumor lesions. This advantage was validated in the Raji

lymphoma and RPMI 8226 MM models. In the systemically disseminated model of Raji—where $CXCR4^+$ malignant cells preferentially colonize CXCL12-rich organs—$CXCR4^{hi}$ CD19 CAR-T cell treatment significantly reduced the $hCD19^+$ tumor burden in liver and bone marrow when compared with second-generation CAR-T cell treatment. Similarly, compared with second-generation BCMA CAR-T cells, $CXCR4^{hi}$ BCMA CAR-T cells also achieved accelerated eradication of disseminated MM cells. These results demonstrated that *CXCR4* modification facilitated the precise tumor tracking and targeted elimination of CAR-T cells in B-cell hematological malignancies. These findings are also supported by previous studies showing that CXCR4 overexpression endows c-kit CAR-T cells and CD33 CAR-CIK cells with increased efficiency of target cell clearance.[42,43]

Bone marrow accumulation was reported to be important for T cell memory formation. It has also been reported that a greater portion of stem cell-like memory T cells in CAR-T cells is correlated with more durable clinical response.[44] This study demonstrated that *CXCR4* modification provided CAR-T cells with enhanced and sustained in vivo protection against B cell lymphoma, primarily by improving their trafficking to tumor sites and bone marrow, as well as promoting memory cell differentiation within the bone marrow niche. We observed that *CXCR4* modification increased the proportions of $CD45RO^+CD62^+T_{CM}$ and $CD45RO^+CD62L^-T_{EM}$ cells in the bone marrow. This finding was corroborated by the GSEA results, which indicated that it was the bone marrow microenvironment, rather than the chemokine CXCL12 alone, conferring CAR-T cells with enhanced memory differentiation. This phenomenon aligns with previous studies showing that $CD8^+$ T cells localize within specialized bone marrow niches, triggering IL-15-dependent homeostatic expansion and facilitating memory precursor-like cell differentiation upon parenchymal entry.[16,37,45–47] In a previous study, high CXCR4 expression was linked to an exhausted phenotype in intratumoral $CD8^+$ T cells.[48] However, the endogenous CXCR4 expression patterns in tumor microenvironment differ fundamentally from those of the ex vivo engineered CAR-T cells with defined CXCR4 overexpression used in this study. As demonstrated by our data, these $CXCR4^{hi}$ CAR-T cells did not exhibit increased T cell exhaustion. In addition, compared with other chemokine receptor-induced homing strategies,[49–51] such as CCR7 and CXCR2, CXCR4 modification not only enhanced CAR-T cells migration to tumor site but also improved their homing to the bone marrow, where they were endowed with enhanced in vivo memory differentiation and persistence.

To date, FDA has approved four CD19 CAR-T cell products (Tisa-cel, Axi-cel, KTE-X19 and Liso-cel) for r/r B cell lymphoma treatment. In pivotal clinical trials, 13.7–21.3% of patients were unable to achieve the best response within the first month.[52–54] The median dosages were 3.0×10^8 CAR^+ T cells (Tisa-cel) in JULIET study, 2×10^6 CAR^+ T cells/kg (Axi-cel) in ZUMA-1 study, and the recommended dose was 1×10^8 CAR^+ T cells (Liso-cel) in TRANSCEND study.[52–54] The real-world study reported by Jain et al. demonstrated similar clinical efficacy,[55] and the proportion of patients who achieved the best response within the first month was comparable to that reported in above mentioned studies. In our study, all 4 patients in low-dose cohort received 1×10^6 CAR^+ T cells/kg, with 3 patients achieving CR and 1 patient achieving PR within the first month, demonstrating the potential advantages of *CXCR4* modification in CAR-T cell design. Moreover, treatment-related toxicity was mild, and no new safety signals were observed. It is currently accepted that the risk factors for CRS include high number and peak expansion of CAR-T cells and the presence of CD28 costimulatory signal.[56] By enhancing tumor tracking and bone marrow homing, *CXCR4* modification actually leads to short-term circulation retention and limited peripheral expansion of CAR-T cells, which potentially reduced the risk of CRS. However, larger clinical trials are warranted to further investigate the safety and efficacy of this approach.

Although our study displayed promising findings, several questions remain to be answered. First, we provided convincing evidence that *CXCR4*-modification enhanced CAR-T cell bone marrow homing and promotes their memory differentiation; however, the underlying mechanisms of memory T cell differentiation in bone marrow require to be further validated in human. Second, current clinical results were based on low-dose cohort of four patients; therefore increased sample size was necessary in further studies to strengthen the findings. Third, although we demonstrated *CXCR4*-modification enhanced CAR-T cell efficacy in B-cell malignancies, the data were based on modification of second-generation CAR-T cells. The versatility of this strategy to universal CAR-T cell platforms and in vivo CAR-T systems is worth further exploration.

In conclusion, we showed that *CXCR4*-modification potentiated the tumor elimination capacity of CD19-targeted and BCMA-targeted CAR-T cells with enhanced in vivo tumor tracking and persistence, which indicates that CXCR4-CXCL12 axis could be utilized for the optimization of CAR-T cell therapies in B cell malignancies, especially for diseases involved bone marrow dissemination.

MATERIALS AND METHODS

Ethics statement

All animal experiments were performed in accordance with the Institutional Animal Care and Use Committee of Sichuan University. The clinical study protocol was approved by the Ethics Committee on Biomedical Research, West China Hospital of Sichuan University (2023 Review (No. 396)), with informed consent obtained from the participants before the study.

Cell lines

The human B cell lymphoma cell lines (Raji, Daudi, and Ramos), multiple myeloma cell lines (RPMI 8226, H929, U266, and OPM2), K562 leukemia cell, and HEK-293T cell were stored in the State Key Laboratory of Biotherapy of Sichuan University. $Raji^{CXCL12}$, $Raji^{luc}$, and $RPMI\ 8226^{luc}$ cells were generated via lentivirus transduction. HEK-293T cells were cultured in DMEM (Gibco), while tumor cells were cultured in RPMI 1640 supplemented with 10% fetal bovine serum (PANTM-Seratach). All the cells were incubated at 37 °C in a humid atmosphere with 5% CO_2. Recombinant human CXCL12 (rhCXCL12) was purchased from Novoprotein.

Lentivirus production and generation of CAR-T cells

All CARs were constructed via the pWPXLd vector backbone (Addgene). The second-generation CD19 CAR was composed of a CD19-specific single-chain variable fragment (scFv, derived from Clone 18, Juno Therapeutic, US10533055B2), an IgG4 hinge and a CD28 transmembrane region, fused with the 4-1BB and CD3ζ intracellular signaling domains. The second-generation BCMA CAR was composed of a BCMA-specific single variable heavy domain of the heavy chain (VHH) (derived from BC817, ABLINK BIOTECH), a CD8 hinge, and a transmembrane region fused with the 4-1BB and CD3ζ intracellular signaling domains. CXCR4-modified CAR-T cells were generated from a tandem construct encoding a second-generation CAR and a human CXCR4 (accession number: NM_001348056), with a P2A peptide sequence between the two genes. For preclinical experiments, lentiviruses and CAR-T cells were prepared as previously described.[57]

Clinical CAR-T-cell manufacture

For clinical use, $CXCR4^{hi}$ CD19 CAR-T cells were manufactured at the Manufacturing Center of Biological Products, West China Hospital, under good manufacturing practice guidelines.

Peripheral blood mononuclear cells were obtained from participating patients who met all screening criteria and underwent leukapheresis. $CD3^+$ T cells were purified (Miltenyi) and activated with anti-CD3/anti-CD28 Dynabeads (Gibco). T cells were subsequently transduced with a lentiviral vector encoding a $CXCR4^{hi}$ CD19 CAR (Hillgene) and expanded ex vivo in OptiVitro® T-cell culture medium (Suzhou Excel Biotechnology Co., Ltd) containing IL-2, IL-7 and IL-15 (Novoprotein) for 11 to 14 days. Rigorous quality control methods, including identity, safety, purity and potency, were used during CAR-T-cell preparation.

Flow cytometry

APC-conjugated anti-human CXCR4 antibody (12G5), FITC-conjugated anti-human CD19 antibody (4G7), and PE-conjugated anti-human BCMA antibody (19F2) were purchased from Biolegend and used to detect the CXCR4, CD19 and BCMA expression levels, respectively. FITC-conjugated human CD19 (ACRO Biosystems) and BCMA proteins (Novoprotein) were used to detect CAR expressions. Brilliant Violet 510-conjugated CD8 (SK1), PE-conjugated CD4 (SK3), PE-conjugated CD45RO (UCHL1), PE-Cy7-conjugated CD62L (DREG-56), PE-Cy7-conjugated PD-1 (A17188B), PE-Cy7-conjugated TIM-3 (F38-2E2), and PE-Cy7-conjugated LAG-3 (11C3C65) antibodies were all purchased from Biolegend. Zombie NIRTM (BioLegend) was used to gate out live/dead cells. Data were acquired with the ACEA NovoCyte flow cytometer, and analysis were performed with NovoExpress software (ACEA Biosciences, version 1.2).

In vitro proliferation assay

Briefly, CAR-T cells were labeled with carboxyfluorescein diacetate succinimidyl ester (CFSE) (CellTrace™ CFSE Cell Proliferation Kit, Invitrogen). Then, T cell stimulation was conducted in coculture with irradiated target cells (12 Gy irradiation, Raji) for 24 h, at an E:T ratio of 1:1. Then, analysis on CFSE dilution was detected by flow cytometry (FITC channel).

Immunofluorescence staining

Immunofluorescence (IF) staining was conducted on formalin-fixed, paraffin-embedded tumor and bone marrow sections. In brief, tissue sections were deparaffinized, rehydrated, and subjected to antigen retrieval. Then, the bone marrow and tumor-infiltrated CAR-T cells were stained with a primary anti-CD3 antibody (SP162, Abcam) and a secondary Opal 570 Red antibody (AKOYA BIOSCIENCES). The quantification of the positively stained region was performed via ImageJ.

IncuCyte internalization assay

An IncuCyte® antibody internalization assay was performed to analyze internalized CXCR4 on the T cell surface. Briefly, an anti-human CXCR4 antibody (Novoprotein) was mixed with IncuCyte® FabFluor-pH Red Antibody Labeling reagent (Sartorius) at a molar ratio of 1:3 in culture medium and incubated for 15 min to obtain an IncuCyte® FabFluor-pH Red-labeled CXCR4 antibody. Then, 1×10^4 T cells were seeded per well into a polyornithine-pretreated 96-well plate, and 24 h later, 50 μL of IncuCyte® FabFluor-pH Red-labeled CXCR4 antibody was added together with 50 μL of lentivirus or culture medium. Images were repeatedly scanned and captured every 15–30 min in an IncuCyte® S3 Live-Cell Analysis System and analyzed via integrated software.

In vitro cytotoxicity assay

The target tumor cells were labeled with CFSE (green) and cocultured with CAR-T cells at different E:T ratios (4:1, 2:1, or 1:1). Twenty-four hours later, residual $CFSE^+$ tumor cells were measured via flow cytometry, and Zombie NIRTM (BioLegend) was used to gate live/dead cells. The cytotoxicity of CAR-T cells is presented as the ratio of live target cells in the coculture group to those in the target cell-only group.

Transwell migration assay

The chemotaxis capacity of CAR-T cells in response to CXCL12 was assessed via a transwell migration assay. CAR-T cells were starved for 12 h before the experiment. Then, 1×10^5 CAR-T cells were added to 200 μL of medium in the upper layer of a transwell unit with a 5 μm polycarbonate filter (Corning), and the lower chamber was loaded with culture medium alone, culture medium containing 100 ng/ml rhCXCL12, or supernatant from $Raji^{CXCL12}$ cells. After 4 h of incubation, the cells in the bottom well were collected and counted. Migration (%) = (cells from the lower chamber/total number of seeded cells) ×100.

Cytokine release assay

CAR-T cells were cocultured with target tumor cells (5×10^3) at the indicated E:T ratios, with 200 μL of culture medium per well (BD Biosciences). Twenty-four hours later, the culture supernatant was harvested for detection of human IFN-γ, TNF-α and IL-2. ELISA was performed according to the manufacturer's protocol (Thermo Fisher).

In vivo antitumor activity

Female B-NDG (NOD. CB17-*Prkdc*^{scid}*IL2rg*^{tm1}/Bcgen) mice aged 6–8 weeks were purchased from Beijing Biocytogen Co., Ltd. In the s.c. tumor model, the mice were injected in the left flank with either 5×10^6 $Raji^{CXCL12}$ or RPMI 8226 cells. When the tumor volume reached ~100 mm^3, the mice were randomly divided into different groups, and CAR-T cells were administered by i.v. infusion. Tumor growth was monitored, and tumor volume was calculated as Length × $Width^2/2$. For the tumor dissemination model, the mice were i.v. injected with either 2×10^6 $Raji^{Luc}$ or RPMI 8226^{Luc} cells. Ten days later, CAR-T cells were i.v. administered. The tumor burden was measured once a week via bioluminescence (BLI) imaging via an IVIS (PerkinElmer), and the flux was analyzed with Living Image software v4.3.1.

Chemokine gene expression analysis

The expression of CCL and CXCL family members (41 genes) was extracted from mRNA-seq data of TCGA Program (https://www.cancer.gov/ccg/research/genome-sequencing/tcga). The expression data were log2 transformed, and their density distribution were visualized using RStudio v1.2.5. The quantile of CXCL12 was determined relative to the expression distribution of all CCL and CXCL genes.

Genome-wide transcriptional profiling

At 30 days after infusion, bone marrow-infiltrated CAR-T cells were isolated from $Raji^{CXCL12}$ s.c. tumor-bearing mice via CD3 MicroBeads (Miltenyi Biotec). The in vitro cultured CAR-T cells were purified similarly after 24 h of stimulation with 12 Gy-irradiated Raji cells (E:T = 1:1), either in the presence or absence of CXCL12 (100 ng/ml). The extracted RNA from $CD3^+$ T cells was sent to Novogene for RNA sequencing via the Agilent Whole Human Genome Oligo Microarray platform. RNA preparation and microarray hybridization were performed according to the manufacturers' instructions. GO enrichment analysis was performed to identify the functional implications of DEGs by characterizing their enrichment in specific GO biological process terms. GSEA was conducted on the dataset employing the MsigDB C7 (immunologic signatures) and MsigDB H (Hallmark) collections.

Patients and study design

An investigator-initiated phase 1 study of autologous $CXCR4^{hi}$ CD19 CAR-T cells was conducted in adults with r/r B cell lymphoma (ClinicalTrials.gov, NCT04684472). The primary endpoint was safety. Eligible patients were adults aged 18–70 years with a histologically confirmed diagnosis of $CD19^+$ B cell lymphoma and an estimated survival time of ≥12 weeks. The patients were required to meet the following conditions:

recurrence or relapse after 2 or more remedial treatments, relapse after autoHSCT or unsuitable for autoHSCT, at least one assessable tumor lesion, an Eastern Cooperative Oncology Group (ECOG) performance status of 0 to 2, a creatinine clearance rate of ≥60 ml/min, alanine transaminase (ALT) and aspartate transaminase (AST) levels ≤2.5 times the upper limit of normal, and a total bilirubin level ≤1.5 times the upper limit of normal. This therapy included 3 days of lymphodepletion chemotherapy combined with fludarabine ($30\,mg\,m^{-2}$ from days −5–3) and cyclophosphamide ($300\,mg\,m^{-2}$ from days −5–3). CAR-T-cell infusion was performed 2 days after the end of lymphodepletion chemotherapy, followed by standard monitoring. Treatment response was assessed according to the revised criteria of the Lugano classification.[58]

Adverse events and follow-ups

CRS and ICANS were evaluated on the basis of Lee and colleagues' 2019 grading criteria, whereas other adverse events (AEs) were assessed and graded according to the National Cancer Institute Common Terminology Criteria for Adverse Events (NCI-CTCAE) version 5.0.[59,60]

CAR copy number analysis by droplet digital PCR (ddPCR)

Patient peripheral blood was collected at the indicated time points. Blood DNA was extracted. The primers used to target the 19bbζ sequence were as follows: forward, 5′-GCTGTAGCTGCCGATTTCCA-3′; reverse, 5′-GGTTCTGGCCCTGCTTGTAC-3′; and probe, 5′-AGTGAAGTTCAGCAGGAGCGCA GACG-3′. Digital PCR was performed via a Quantalife QX200 Droplet Digital PCR system (Bio-Rad). Droplets were generated in a DG8 cartridge via a QX200 droplet generator (Bio-Rad). The water-in-oil emulsions were pipette transferred to a 96-well polypropylene plate (Bio-Rad), which was sealed via a PX1 sealing instrument. The PCR amplification was performed under the following conditions: 95 °C for 10 min, 94 °C for 30 s, 60 °C for 1 min (40 cycles, 2 °C/s ramp rate), followed by a 10-min hold at 98 °C, and a final hold at 4 °C. Subsequently, the amplified products were subjected to droplet using a QX200 droplet reader (Bio-Rad). The resulting ddPCR data were analyzed with QuantaSoft software version 1.7.4 (Bio-Rad) in accordance with the manufacturers' protocol. Reaction-specific thresholds were set for the FAM channel and manually optimized as needed. The droplet reader software results are presented as copies/μL for the CAR. CAR copies per μg gDNA = (Copies concentration (copies/μL) × 20/100 ng × 1000).

Statistical analysis

Statistical analysis was performed via the Prism software package (GraphPad, San Diego, CA), and all the data are presented as the means ± SDs. Significant differences were analyzed by two-sided unpaired Student's *t* test, one-way ANOVA, or the log-rank test. $p < 0.05$ was considered significant.

DATA AVAILABILITY

The RNA-seq datasets generated in this study are available in the GEO repository under accession numbers GSE305737 (in vivo) and GSE305732 (in vitro). All data supporting the findings of this study are included in the submitted material. Upon reasonable request, and subject to criteria, conditions, and exceptions, the corresponding author will provide access to individual de-identified participant data.

ACKNOWLEDGEMENTS

This study was supported by the National Science and Technology Major Project (2018ZX09733001-003-004), the National Natural Science Foundation of China (82272795), the CAMS Innovation Fund for Medical Sciences (CIFMS, 2021-I2M-C&T-A-024), the Sichuan Science and Technology Program (2023YFS0003), the 1·3·5 project for disciplines of excellence–Clinical Research Fund, West China Hospital, Sichuan University (2023HXFH003), and the Institutional Research Fund of Sichuan University (2022SCUH0034). We express our gratitude to the study patients and their families.

AUTHOR CONTRIBUTIONS

Y.S.W. conceptualized the idea of this study. P.S., F.C.G., L.Q.Z., and D.L. designed the study; P.S., F.C.G., D.Y.Q., Q.Z.M., B.X.Z., G. G., Y.C., and X.H. performed most of the in vitro and in vivo experiments. P.S. and D.Y.Q. performed the data analysis. N.L., K.X.Z., and X.Y.L. helped carry out the in vitro experiments. N.L., K.X.Z., J.Z., X.Y.L., and Y.G. helped carry out the in vivo experiments. Y.G.Z., Y.Z., and M.Y.F. helped with the interpretation of the data. L.Q.Z. and M.J. helped to conduct the clinical trial. P. S. and D.Y.Q. drafted the manuscript. D.L. and Y.S.W. revised and edited the manuscript. All the authors have read and approved the article.

ADDITIONAL INFORMATION

Supplementary information The online version contains supplementary material available at https://doi.org/10.1038/s41392-025-02522-2.

Competing interests: The authors declare no competing interests.

Publisher's note Springer Nature remains neutral with regard to jurisdictional claims in published maps and institutional affiliations.

REFERENCES

1. Cyster, J. G. Chemokines and cell migration in secondary lymphoid organs. *Science* **286**, 2098–2102 (1999).
2. Li, H. et al. Targeting brain lesions of non-small cell lung cancer by enhancing CCL2-mediated CAR-T cell migration. *Nat. Commun.* **13**, 2154 (2022).
3. Cadilha, B. L. et al. Combined tumor-directed recruitment and protection from immune suppression enable CAR T cell efficacy in solid tumors. *Sci. Adv.* **7**, 5781 (2021).
4. Jin, L. et al. Enhance anti-lung tumor efficacy of chimeric antigen receptor-T cells by ectopic expression of C-C motif chemokine receptor 6. *Sci. Bull.* **66**, 803–812 (2021).
5. Jin, L. et al. CXCR1- or CXCR2-modified CAR T cells co-opt IL-8 for maximal antitumor efficacy in solid tumors. *Nat. Commun.* **10**, 4016 (2019).
6. Blades, M. C. et al. Stromal cell-derived factor 1 (CXCL12) induces human cell migration into human lymph nodes transplanted into SCID mice. *J. Immunol.* **168**, 4308–4317 (2002).
7. Cambier, S., Gouwy, M. & Proost, P. The chemokines CXCL8 and CXCL12: molecular and functional properties, role in disease and efforts towards pharmacological intervention. *Cell Mol. Immunol.* **20**, 217–251 (2023).
8. Venetz, D. et al. Perivascular expression of CXCL9 and CXCL12 in primary central nervous system lymphoma: T-cell infiltration and positioning of malignant B cells. *Int. J. Cancer* **127**, 2300–2312 (2010).
9. Arai, J. et al. Stromal cells in lymph nodes attract B-lymphoma cells via production of stromal cell-derived factor-1. *Eur. J. Haematol.* **64**, 323–332 (2000).
10. Vande Broek, I. et al. Clinical significance of chemokine receptor (CCR1, CCR2 and CXCR4) expression in human myeloma cells: the association with disease activity and survival. *Haematologica* **91**, 200–206 (2006).
11. Pals, S. T., de Gorter, D. J. & Spaargaren, M. Lymphoma dissemination: the other face of lymphocyte homing. *Blood* **110**, 3102–3111 (2007).
12. Ullah, T. R. The role of CXCR4 in multiple myeloma: Cells' journey from bone marrow to beyond. *J. Bone Oncol.* **17**, 100253 (2019).
13. Singh, N. et al. Early memory phenotypes drive T cell proliferation in patients with pediatric malignancies. *Sci. Transl. Med.* **8**, 320ra323 (2016).
14. Chen, G. M. et al. Integrative bulk and single-cell profiling of premanufacture T-cell populations reveals factors mediating long-term persistence of CAR T-cell therapy. *Cancer Discov.* **11**, 2186–2199 (2021).
15. Maude, S. L. et al. Chimeric antigen receptor T cells for sustained remissions in leukemia. *N. Engl. J. Med.* **371**, 1507–1517 (2014).
16. Khan, A. B. et al. Redirection to the bone marrow improves T cell persistence and antitumor functions. *J. Clin. Invest.* **128**, 2010–2024 (2018).
17. Di Rosa, F. Two niches in the bone marrow: a hypothesis on life-long T cell memory. *Trends Immunol.* **37**, 503–512 (2016).
18. Mazo, I. B. et al. Bone marrow is a major reservoir and site of recruitment for central memory CD8+ T cells. *Immunity* **22**, 259–270 (2005).
19. Alsayed, Y. et al. Mechanisms of regulation of CXCR4/SDF-1 (CXCL12)-dependent migration and homing in multiple myeloma. *Blood* **109**, 2708–2717 (2007).
20. Middle, S. et al. Immunohistochemical analysis indicates that the anatomical location of B-cell non-Hodgkin's lymphoma is determined by differentially expressed chemokine receptors, sphingosine-1-phosphate receptors and integrins. *Exp. Hematol. Oncol.* **4**, 10 (2015).
21. Recasens-Zorzo, C. et al. Pharmacological modulation of CXCR4 cooperates with BET bromodomain inhibition in diffuse large B-cell lymphoma. *Haematologica* **104**, 778–788 (2019).

22. Contento, R. L. et al. CXCR4-CCR5: a couple modulating T cell functions. *Proc. Natl Acad. Sci. USA* **105**, 10101–10106 (2008).
23. Bermejo, M. et al. Activation of blood T lymphocytes down-regulates CXCR4 expression and interferes with propagation of X4 HIV strains. *Eur. J. Immunol.* **28**, 3192–3204 (1998).
24. Abbal, C. et al. TCR-mediated activation of allergen-specific CD45RO(+) memory T lymphocytes results in down-regulation of cell-surface CXCR4 expression and a strongly reduced capacity to migrate in response to stromal cell-derived factor-1. *Int. Immunol.* **11**, 1451–1462 (1999).
25. Nian, Z. et al. Rapamycin pretreatment rescues the bone marrow AML cell elimination capacity of CAR-T cells. *Clin. Cancer Res.* **27**, 6026–6038 (2021).
26. Johnson, N. M. et al. HIV-based lentiviral vectors: origin and sequence differences. *Mol. Ther. Methods Clin. Dev.* **21**, 451–465 (2021).
27. Choi, B. et al. Down-regulation of cell surface CXCR4 by HIV-1. *Virol. J.* **5**, 6 (2008).
28. Sloan, R. D. et al. Expression of Nef from unintegrated HIV-1 DNA downregulates cell surface CXCR4 and CCR5 on T-lymphocytes. *Retrovirology* **7**, 44 (2010).
29. Toyoda, M. et al. Differential ability of primary HIV-1 Nef isolates to downregulate HIV-1 entry receptors. *J. Virol.* **89**, 9639–9652 (2015).
30. Hidalgo-Estévez, A. M. et al. HIV-1-Tat potentiates CXCL12/stromal cell-derived factor 1-induced downregulation of membrane CXCR4 in T lymphocytes through protein kinase C zeta. *Mol. Immunol.* **46**, 106–115 (2008).
31. Valiathan, R. R. & Resh, M. D. Differential control of CXCR4 and CD4 down-regulation by HIV-1 Gag. *Virol. J.* **5**, 23 (2008).
32. Montalvo, M. J. et al. Decoding the mechanisms of chimeric antigen receptor (CAR) T cell-mediated killing of tumors: insights from granzyme and Fas inhibition. *Cell Death Dis.* **15**, 109 (2024).
33. Peled, A. et al. Dependence of human stem cell engraftment and repopulation of NOD/SCID mice on CXCR4. *Science* **283**, 845–848 (1999).
34. Moreno, M. J. et al. CXCR4 expression enhances diffuse large B cell lymphoma dissemination and decreases patient survival. *J. Pathol.* **235**, 445–455 (2015).
35. Goedhart, M. et al. CXCR4, but not CXCR3, drives CD8(+) T-cell entry into and migration through the murine bone marrow. *Eur. J. Immunol.* **49**, 576–589 (2019).
36. Nakayama, T. et al. Cutting edge: profile of chemokine receptor expression on human plasma cells accounts for their efficient recruitment to target tissues. *J. Immunol.* **170**, 1136–1140 (2003).
37. Sercan Alp, Ö et al. Memory CD8(+) T cells colocalize with IL-7(+) stromal cells in bone marrow and rest in terms of proliferation and transcription. *Eur. J. Immunol.* **45**, 975–987 (2015).
38. Alp, ÖS. & Radbruch, A. The lifestyle of memory CD8(+) T cells. *Nat. Rev. Immunol.* **16**, 271 (2016).
39. Sehgal, A. et al. Lisocabtagene maraleucel as second-line therapy in adults with relapsed or refractory large B-cell lymphoma who were not intended for haematopoietic stem cell transplantation (PILOT): an open-label, phase 2 study. *Lancet Oncol.* **23**, 1066–1077 (2022).
40. Labanieh, L. & Mackall, C. L. CAR immune cells: design principles, resistance and the next generation. *Nature* **614**, 635–648 (2023).
41. Pansy, K. et al. The CXCR4-CXCL12-axis is of prognostic relevance in DLBCL and its antagonists exert pro-apoptotic effects in vitro. *Int. J. Mol. Sci.* **20**, 4740 (2019).
42. Arai, Y. et al. Myeloid conditioning with c-kit-targeted CAR-T cells enables donor stem cell engraftment. *Mol. Ther.* **26**, 1181–1197 (2018).
43. Biondi, M. et al. Selective homing of CAR-CIK cells to the bone marrow niche enhances control of the acute myeloid leukemia burden. *Blood* **141**, 2587–2598 (2023).
44. Ouyang, W. et al. PD-1 downregulation enhances CAR-T cell antitumor efficiency by preserving a cell memory phenotype and reducing exhaustion. *J. Immunother. Cancer* **12**, 8429 (2024).
45. Ku, C. C. et al. Control of homeostasis of CD8+ memory T cells by opposing cytokines. *Science* **288**, 675–678 (2000).
46. Grabstein, K. H. et al. Cloning of a T cell growth factor that interacts with the beta chain of the interleukin-2 receptor. *Science* **264**, 965–968 (1994).
47. Chaix, J. et al. Cutting edge: CXCR4 is critical for CD8+ memory T cell homeostatic self-renewal but not rechallenge self-renewal. *J. Immunol.* **193**, 1013–1016 (2014).
48. Cao, C. et al. CXCR4 orchestrates the TOX-programmed exhausted phenotype of CD8(+) T cells via JAK2/STAT3 pathway. *Cell Genom.* **4**, 100659 (2024).
49. Schomer, N. T. et al. CCR7 expression in CD19 chimeric antigen receptor-engineered natural killer cells improves migration toward CCL19-expressing lymphoma cells and increases tumor control in mice with human lymphoma. *Cytotherapy* **24**, 827–834 (2022).
50. Whilding, L. M. et al. CAR T-cells targeting the integrin αvβ6 and co-expressing the chemokine receptor CXCR2 demonstrate enhanced homing and efficacy against several solid malignancies. *Cancers* **11**, 674 (2019).
51. Maalej, K. M. et al. CAR-cell therapy in the era of solid tumor treatment: current challenges and emerging therapeutic advances. *Mol. Cancer* **22**, 20 (2023).
52. Schuster, S. J. et al. Tisagenlecleucel in adult relapsed or refractory diffuse large B-cell lymphoma. *N. Engl. J. Med.* **380**, 45–56 (2019).
53. Neelapu, S. S. et al. Axicabtagene ciloleucel CAR T-cell therapy in refractory large B-cell lymphoma. *N. Engl. J. Med.* **377**, 2531–2544 (2017).
54. Abramson, J. S. et al. Lisocabtagene maraleucel for patients with relapsed or refractory large B-cell lymphomas (TRANSCEND NHL 001): a multicentre seamless design study. *Lancet* **396**, 839–852 (2020).
55. Jain, M. D. et al. Five-year follow-up of standard-of-care axicabtagene ciloleucel for large B-cell lymphoma: results from the US lymphoma CAR T consortium. *J. Clin. Oncol.* **42**, 3581–3592 (2024).
56. Schubert, M. L. et al. Side-effect management of chimeric antigen receptor (CAR) T-cell therapy. *Ann. Oncol.* **32**, 34–48 (2021).
57. Ma, Q. et al. A PD-L1-targeting chimeric switch receptor enhances efficacy of CAR-T cell for pleural and peritoneal metastasis. *Signal Transduct. Target Ther.* **7**, 380 (2022).
58. Cheson, B. D. et al. Recommendations for initial evaluation, staging, and response assessment of Hodgkin and non-Hodgkin lymphoma: the Lugano classification. *J. Clin. Oncol.* **32**, 3059–3068 (2014).
59. Lee, D. W. et al. ASTCT consensus grading for cytokine release syndrome and neurologic toxicity associated with immune effector cells. *Biol. Blood Marrow Transpl.* **25**, 625–638 (2019).
60. Lee, D. W. et al. Current concepts in the diagnosis and management of cytokine release syndrome. *Blood* **124**, 188–195 (2014).